Theta oscillations in anterior cingulate cortex and orbitofrontal cortex differentially modulate accuracy and speed in flexible reward learning

Running Title: *Frontal cortex theta in flexible learning*

Tony Ye[1], Juan Luis Romero-Sosa[1], Anne Rickard[1], Claudia G. Aguirre[1], Andrew M. Wikenheiser[1-4], Hugh T. Blair[1-3], and Alicia Izquierdo*[1-4]

[1] Department of Psychology, UCLA, Los Angeles, CA 90095, USA
[2] The Brain Research Institute, UCLA, Los Angeles, CA 90095, USA
[3] Integrative Center for Learning and Memory, UCLA, Los Angeles, CA 90095, USA
[4] Integrative Center for Addictions, UCLA, Los Angeles, CA 90095, USA

Author contributions: TY and AI designed the research; TY, AR, and AI performed the research; TY, JLRS, CGA, HTB, and AI analyzed the data; TY, AMW, HTB, and AI interpreted the data; HTB and AI acquired funding for the project; TY and AI wrote the paper; TY, JLRS, HTB, AMW, and AI edited the final version.

Acknowledgements: This work was supported by UCLA's Division of Life Sciences Retention fund (Izquierdo), R01 DA047870 (Izquierdo and Soltani), R21 MH122800 (Izquierdo and Blair), the Training program in Neurotechnology Translation T32 NS115753 (Ye). We appreciate early and helpful comments from members of the Izquierdo lab on these data. We acknowledge the Staglin Center for Brain and Behavioral Health for additional support related to fluorescence microscopy. We thank Alexandra Stolyarova for help with immunohistochemistry. We also thank the NIDA Drug Supply program for the supply of clozapine-N-oxide.

Correspondence: *Alicia Izquierdo, Ph.D. email: aizquie@psych.ucla.edu Ph: +1 310 825 3459

Manuscript Information:
Pages 41
Figures 7 Supplementary Figures 7

Words: Abstract 216
Intro 729
Discussion 1312

ABSTRACT

Flexible reward learning relies on frontal cortex, with substantial evidence indicating that anterior cingulate cortex (ACC) and orbitofrontal cortex (OFC) subregions play important roles. Recent studies in both rat and macaque suggest theta oscillations (5-10 Hz) may be a spectral signature that coordinates this learning. However, network-level interactions between ACC and OFC in flexible learning remain unclear. We investigated the learning of stimulus-reward associations using a combination of simultaneous *in-vivo* electrophysiology in dorsal ACC and ventral OFC, partnered with bilateral inhibitory DREADDs in ACC. In freely-behaving male and female rats and using a within-subject design, we examined accuracy and speed of response across distinct and precisely-defined trial epochs during initial visual discrimination learning and subsequent reversal of stimulus-reward contingencies. Following ACC inhibition there was a propensity for random responding in early reversal learning, with correct vs. incorrect trials distinguished only from OFC, not ACC, theta power differences in the reversal phase. ACC inhibition also hastened incorrect choices during reversal. This same pattern of change in accuracy and speed was not observed in viral control animals. Thus, characteristics of impaired reversal learning following ACC inhibition are poor deliberation and weak theta signaling of accuracy in this region. The present results also point to OFC theta oscillations as a prominent feature of reversal learning, unperturbed by ACC inhibition.

Keywords: **reversal learning, oscillations, prefrontal cortex, theta, DREADDs**

INTRODUCTION

Both humans and nonhumans alike make a multitude of choices based on adaptations to their environment in order to maximize rewards while minimizing losses. This type of flexible reward learning is thought to rely on the prefrontal cortex. Substantial evidence in primates indicates that anterior cingulate cortex (ACC) and orbitofrontal cortex (OFC) have essential roles in learning about actions and stimuli, respectively (Rudebeck, Behrens et al. 2008, Camille, Tsuchida et al. 2011, Luk and Wallis 2013). Though primate and rodent ACC and OFC are not equivalent structures, we may still learn fundamental principles of their functions in the rodent (Rudebeck and Izquierdo 2021). A mechanistic investigation of their interaction in stimulus-based learning is missing in the broader literature.

Lesion or inhibition of OFC impairs multiple forms of reward learning and in rats this has most extensively been observed in the reversal phase (Chudasama and Robbins 2003, Izquierdo, Darling et al. 2013), particularly in spatial- or action-based reversal learning (Boulougouris, Dalley et al. 2007, Riceberg and Shapiro 2012, Dalton, Wang et al. 2016, Groman, Keistler et al. 2019). Classic recording studies in rat OFC during (olfactory cue) reversal learning (Schoenbaum, Chiba et al. 1999) show that neural activity represents an integration of the motivational significance of a reward and its specific predictive cue, critical for reversal but not discrimination learning (Schoenbaum, Chiba et al. 1999, Marquardt, Sigdel et al. 2017). Conversely, lesion or inhibition of ACC results in decrements in (visual) discrimination performance (Chudasama, Passetti et al. 2003), but has no effect on fully-predictive, deterministic reversal learning (Bussey, Muir et al. 1997, Schweimer and Hauber 2006). Yet ACC neurons in rats integrate motor-related information with expectations of future outcomes (Cowen, Davis et al. 2012, Hyman, Holroyd et al. 2017), encode choice value (Mashhoori, Hashemnia et al. 2018) and maintain trial-by-trial performance (Akam, Rodrigues-Vaz et al. 2021), all processes that would be vital not just to action-based learning but also to stimulus-based reversal learning. This growing body of evidence supports a general role for ACC in maintaining a model about the reward environment and making predictions about future choices associated with either actions or stimuli.

More importantly, how these two regions interact is unclear. Several groups have recorded single-unit and local-field activity simultaneously in both areas and uncovered

overlapping functions, in contrast to the interference studies (Rudebeck, Walton et al. 2006, Rudebeck, Behrens et al. 2008). For example, there is reported evidence of ACC-OFC task-related coherence in theta to low beta (4-20 Hz) oscillations as rats respond to or choose a higher-valued reward, suggesting a functional connectivity underlying relative reward value (Fatahi, Haghparast et al. 2018, Fatahi, Ghorbani et al. 2020, Amarante and Laubach 2021). It is therefore conceivable that these two regions work in a complementary manner for reward-based learning and choice (Hunt and Hayden 2017, Hunt, Malalasekera et al. 2018) potentially with theta oscillations in OFC coordinating reward signals (Marquardt, Sigdel et al. 2017, Knudsen and Wallis 2020) with ACC (Fatahi, Haghparast et al. 2018). However, network-level interactions and the spectral signatures in flexible reward learning remain unclear.

Given that ACC is densely innervated by regions involved not only in evaluating options but also preparing and executing actions, we hypothesized that ACC theta modulates overall learning of stimuli. To test this, we investigated learning using a combination of simultaneous *in-vivo* electrophysiology in dorsal ACC (dorsal area 32/24, van Heukelum, Mars et al. (2020)) and ventral OFC, partnered with inhibitory Designer Receptors Exclusively Activated by Designer Drugs (DREADDs) in ACC. We recorded from posterior VO as it is richly interconnected with ACC (Hoover and Vertes 2011, Barreiros, Panayi et al. 2021). Additionally, a thorough consideration of both accuracy and speed of response during learning may be particularly informative when identifying neural signatures of flexible learning (Aguirre, Stolyarova et al. 2020, Harris, Aguirre et al. 2021), so we include analysis of both here.

We found that ACC inhibition during the discrimination phase had no functional impact on initial performance. In contrast, ACC inhibition in early reversal learning promoted a random response strategy, disrupted ACC signaling of correct vs. incorrect trials, and hastened speed of incorrect choices. The same pattern was not observed in viral control animals. Though ACC inhibition produced these changes in accuracy and speed in the reversal phase, it did not affect OFC theta signaling of accuracy in reversal learning, suggesting an independent process in OFC.

RESULTS

ACC inhibition in early, not late, reversal learning promotes random responding

Fifteen rats were prepared with either inhibitory (hM4Di) DREADDs (n=8, 4 females) or enhanced Green Fluorescent Protein (eGFP) null virus (n=7, 3 females) on putative projection neurons in ACC. Eight of these animals (n=4 hM4Di, n=4 eGFP) were also implanted with custom-constructed 16-channel fixed electrode arrays unilaterally in ACC and OFC, in the same surgery as virus infusion. All rats were tested using a within-subject design for drug administration (**Figure 1**). Rats were administered clozapine-N-oxide (CNO) once they reached criterion-level

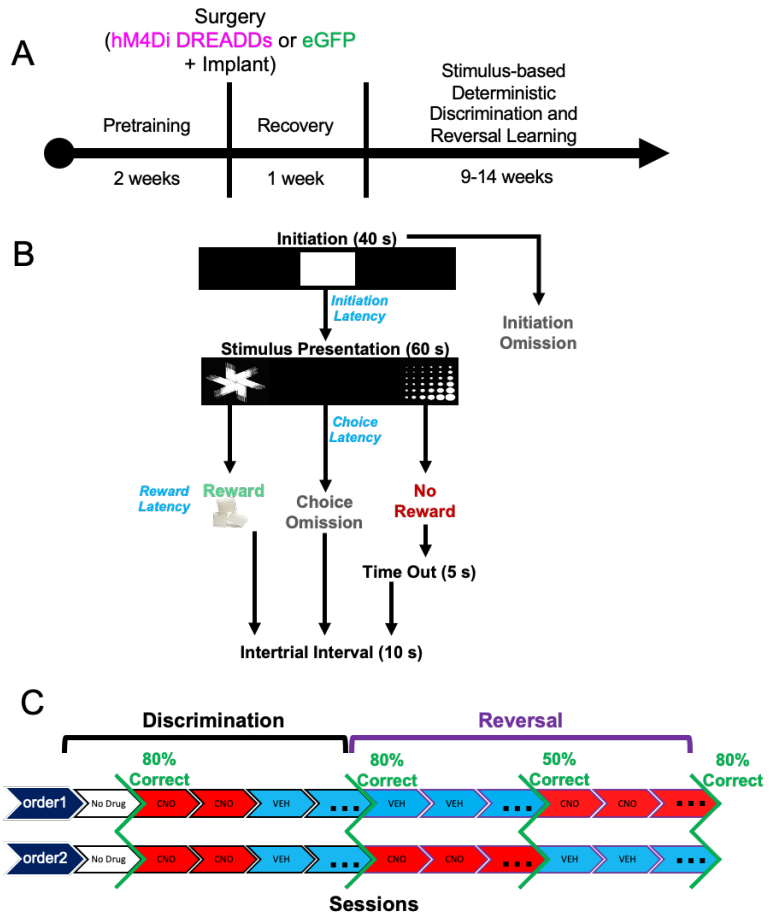

Figure 1. Experimental timeline, task structure, and drug administration. (**A**) After approximately 2 weeks of pretraining, rats underwent bilateral viral infusion of inhibitory hM4Di DREADDs or null virus enhanced Green Fluorescent Protein (eGFP) in ACC along with chronic implantation of electrode arrays targeting both ACC and OFC unilaterally in each animal. (**B**) Following a 1-week recovery period, rats commenced the stimulus-based visual discrimination and reversal learning task, with rewarded-stimulus assignment (e.g., "fan" vs. "marbles") counterbalanced across rats. (**C**) Drug administration (clozapine-N-oxide, CNO or vehicle, VEH) was administered once criterion was reached for initial discrimination to probe the effect of ACC inhibition on mastery-level discrimination performance. Subsequently, in the reversal phase, the order of drug administration was counterbalanced across animals.

127 performance (80%) on the initial discrimination learning phase to assess the impact of ACC
128 inhibition on mastery-level performance (Bussey, Muir et al. 1997, Chudasama, Passetti et al.
129 2003). Subsequently in the reversal phase, they were administered CNO or vehicle (VEH) in
130 counterbalanced order: CNO administered early in learning (to 50% correct) then switched to
131 VEH until 80%, or vice versa (VEH to 50%, then CNO to 80%). We used a CNO dose for ACC
132 inhibition that has previously resulted in behavioral effects on two different reward learning
133 tasks (Stolyarova, Rakhshan et al. 2019, Hart, Blair et al. 2020), and within the dose-range exerting
134 the least off-target effects (Jendryka, Palchaudhuri et al. 2019).

135 There was no significant difference between hM4Di and eGFP animals in initial
136 discrimination learning, though two rats from each virus group failed to learn (sessions to
137 criterion: t(11)= -0.250, *p*=0.807), **Figure 2A**. A mixed-effects GLM was used to analyze probability
138 correct, with drug, virus, and sex as between-subject factors, session as a within-subject factor,
139 and individual rat as random factor. There was no functional consequence of ACC inhibition on
140 mastery level performance (i.e., no significant effect of drug, virus, or interaction of drug x virus
141 in a mixed-effects GLM; GLM formula: $\gamma \sim [1 + Drug*Session*Virus*Sex + (1 + Session | Rat)]$, **Figure**
142 **2B**. A significant effect of session, and interactions of session x virus, and session x virus x drug
143 were observed, **Table 1**. When post-hoc Bonferroni post-hoc comparisons were conducted, we
144 found eGFP ($p<0.01$) but not hM4Di ($p=0.11$) groups decreased in probability across session,
145 though VEH performance was greater than CNO in both eGFP and hM4Di groups (both $p<0.01$s).

146 In contrast to the acquisition curves that demonstrated mastery of the initial visual
147 discrimination, all animals exhibited difficulty learning reversals, rarely achieving above 60%
148 after 10 sessions (**Figure 2C**), similar to a recent report (Harris, Aguirre et al. 2021). A mixed-
149 effects GLM was also used to analyze reversal learning. This analysis resulted in a significant
150 drug x virus interaction ($\beta_{drug\ x\ virus}$ = 0.258, t(178) = 2.56, *p*=0.01). Post-hoc Bonferroni-corrected
151 tests revealed a nonsignificant effect of drug in the hM4Di group (*p*=0.07) and in the eGFP group
152 (*p*=1.0). There were other interactions with sex and session that did not result in significant effects
153 with Bonferroni-corrected post-hoc follow-up (**Table 2**). However, when we added drug order to
154 the GLM model we found a significant drug x drug order interaction ($\beta_{drug\ x\ drug\ order}$ = -0.56983,
155 t(162) = -3.39, *p*<0.001) with an effect of drug only in the hM4Di group (post-hoc Bonferroni-

corrected tests: p=0.01 for hM4Di, p=0.68 for eGFP). Early inhibition of ACC in the reversal phase brought performance to chance and maintained it there (**Figure 2D**), in contrast to rats given VEH first which instead showed the expected tendency to follow the previous stimulus-reward assignment on early reversal sessions during VEH (i.e., more perseveration), but reached higher accuracy levels later, even when administered CNO. Interestingly, CNO had the opposite effect in eGFP animals: when administered early, rats exhibited the expected learning trajectory, but when administered CNO at 50% accuracy, performance remained at chance level (**Figure 2C**). Collectively, the pattern of results reveals a differential effect of CNO in hM4Di and eGFP animals, with ACC inhibition producing a random response strategy early in reversal learning.

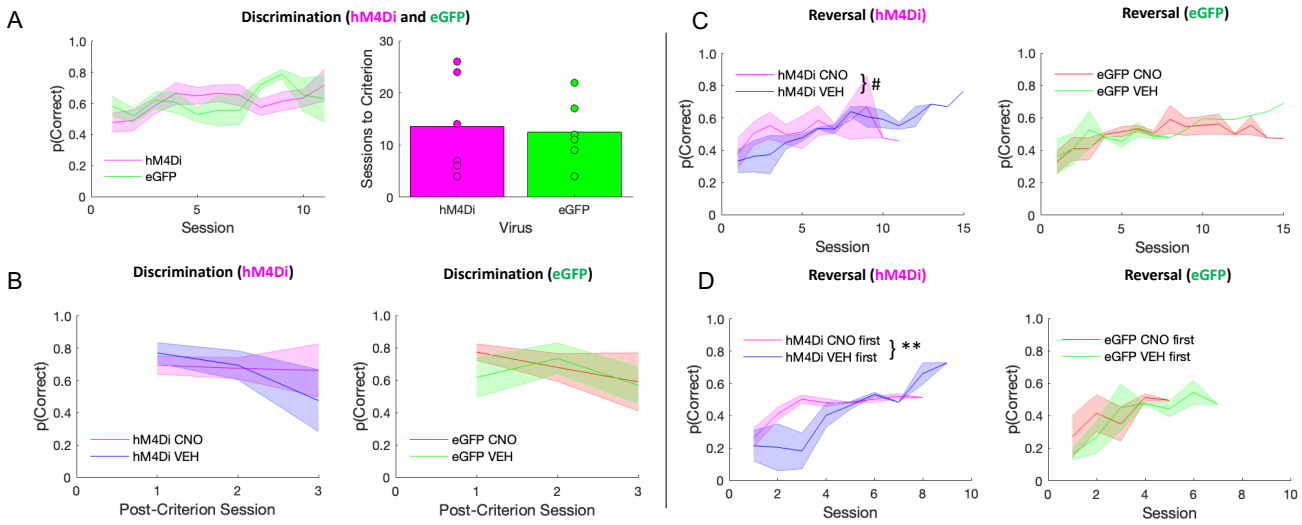

Figure 2. ACC inhibition has no effect on discrimination performance, but promotes random responding during early reversal learning. There were no differences between hM4Di and eGFP virus groups in the initial discrimination phase, however, clozapine-N-oxide (CNO) affected long-term reversal learning differently depending on virus group, and depending on when CNO was administered. **(A)** Performance in hM4Di rats and eGFP rats during initial discrimination of stimuli during which there was no recording and no drug administered (*left*). Rats did not differ by virus group in the number of sessions to reach criterion (*right*). **(B)** There was no difference between virus groups or by drug in post-criterion discrimination performance. **(C)** Learning curves during the reversal phase split by hM4Di (*left*) and eGFP (*right*). Irrespective of virus condition, rats rarely surpassed 60% accuracy. **(D)** Rats received either VEH or CNO first during the reversal phase prior to reaching 50% correct. Same learning as in C, but learning curves now split by whether rats received CNO first or VEH first. ACC inhibition during early reversal learning promotes a random response strategy that they do not recover from. Means ± standard error of the mean (S.E.M.) shades. Post-hoc Bonferroni comparisons, #p=0.07, **p=0.001. hM4Di n=8 (4 female), and eGFP n=7 (3 female).

ACC inhibition attenuates a trial accuracy theta signal in OFC during discrimination

In a subset of learners, we collected local field potential (LFP) data in ACC and OFC (**Figure 3**), acquired at 30 kHz and down sampled to 1,000 Hz, and bandpass filtered for theta (5-

169 10 Hz). We were primarily interested in measures of accuracy: correct vs. incorrect trials (Harris,
170 Aguirre et al. (2021), but we also included trial initiation and reward collection latencies in our
171 analyses. The latter measures did not emerge as significant correlates or predictors of learning.

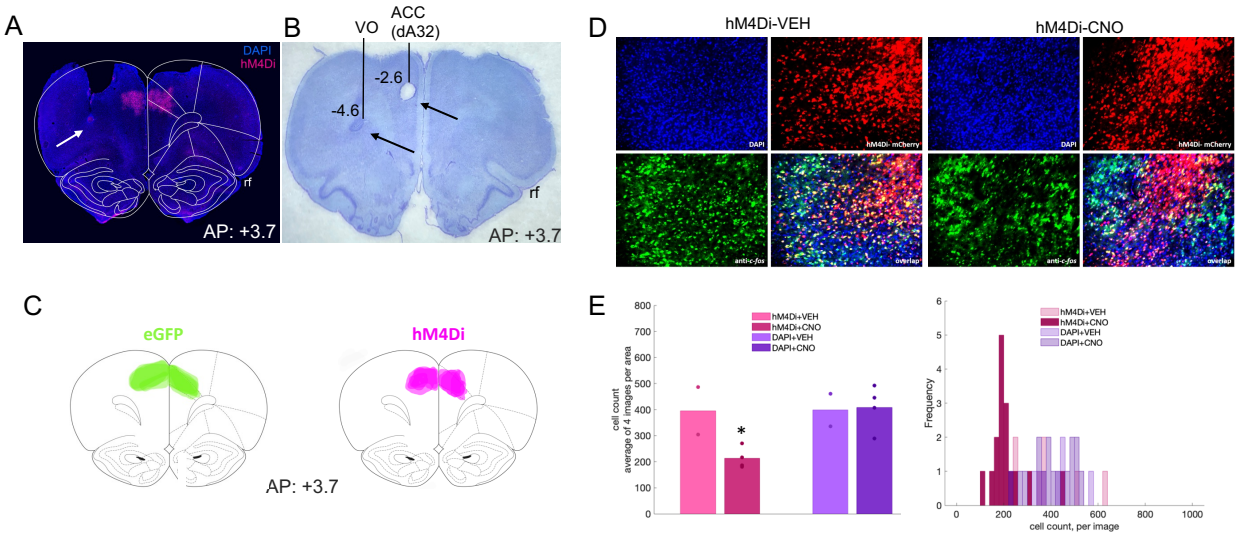

Figure 3. Inhibitory DREADDs in ACC, electrode placement in ACC and OFC, and validation of inhibition in ACC via c-fos immunohistochemistry. **(A)** Representative placement of inhibitory hM4Di DREADDs at Anterior-Posterior (AP) level +3.7 relative to Bregma. Note, tissue (secondary motor cortex, M2) was removed at time of brain extraction. White arrow pointing at tip of electrode track in OFC. **(B)** Nissl-stained section showing electrolytic lesions and placement of electrode arrays targeting both ACC (dorsal area 32, dA32) and OFC (ventral orbital, VO) unilaterally in a representative animal. Black arrows pointing at tip of electrode tracks. rf = rhinal fissure. **(C)** Reconstructions of placement of inhibitory hM4Di DREADDs (right) and eGFP null virus (left) at Anterior-Posterior (AP) level +3.7 relative to Bregma. **(D)** Representative DAPI, hM4Di-mCherry, c-fos immunoreactivity and their overlap after injections of VEH (left) or CNO (right). **(E)** Mean cell count of 4 images per condition, hM4Di+VEH, hM4Di+CNO, DAPI+VEH, and DAPI+CNO. One-way ANOVA resulted in a significant decrease in c-fos positive cells in the hM4Di-expressing areas, but not in the DAPI areas (left). Histogram of cell count frequency for each image by condition (right). *p<0.05.

172

173 Based on the temporal profile of theta power changes during behavior in animals
174 transfected with hM4Di (**Figure S2)** and eGFP in ACC (**Figure S3**), we baseline-subtracted theta
175 band in ACC and OFC using the immediate pre-event period (-200 ms) leading up to the choice
176 of the correct or incorrect stimulus. This was the moment at which the animal had already
177 initiated a trial, and was fixating on the stimulus of choice. We calculated this for both
178 discrimination and reversal phases. Despite no performance decrements following ACC
179 inhibition in discrimination learning, normalized theta power in ACC during both correct and
180 incorrect trials was significantly lower after CNO than after VEH in hM4Di animals (**Figure 4A**).
181 We performed 2 x 2 ANOVAs on this baseline-subtracted theta power comparing trial type
182 (correct, incorrect) and drug (VEH, CNO) for discrimination sessions, separately for OFC and

ACC. In ACC, we observed a significant effect of trial type [$F(1,45)=14.237$, $p<0.0001$] and a significant drug x trial type interaction [$F(1,45)=5.859$, $p=0.02$], with increases in ACC theta in both correct and incorrect trials in the VEH compared to the CNO condition (Bonferroni-corrected post-hoc comparisons, all $p<0.035$). There was no such pattern for normalized OFC theta during discrimination, and there was a nonsignificant effect of drug [$F(1,50)=3.965$, $p=0.052$] (**Figure 4B**). In animals with eGFP virus, one could distinguish correct from incorrect trials from normalized theta in OFC [trial type x drug: $F(1,27)=6.940$, $p=0.01$, Bonferroni-corrected post-hoc comparisons, all $p<0.01$], but not in ACC. In sum, ACC inhibition attenuated a trial accuracy theta signal in OFC during discrimination (**Figure 4B** when compared to **Figure 4D**), but these changes did not appreciably impact accurate performance.

Correct vs. incorrect trials are strongly differentiated by OFC, but not ACC, theta power in the reversal phase following ACC inhibition

Following ACC inhibition, correct vs. incorrect trials in reversal learning could only be distinguished by OFC, not ACC, normalized theta. As above, we performed two separate 2 x 2 ANOVAs, comparing trial type (correct, incorrect) and drug (VEH, CNO) for all reversal sessions, separately for OFC and ACC. In hM4Di animals, there was a main effect of trial type on normalized OFC theta in reversal [$F(1,143)=51.250$, $p<0.0001$, all corrected Bonferroni post-hoc comparisons of correct vs. incorrect trials, all $p<0.001$] (**Figure 4B**). This difference by trial type in normalized theta power was absent in ACC, in the hM4Di animals. In eGFP animals, there was a significant effect of trial type for normalized OFC theta [$F(1,132)=6.21$, $p<0.01$] and ACC theta [$F(1,132)=6.109$, $p=0.01$], with post-hoc Bonferroni-corrected comparisons revealing normalized theta was greater for correct choices compared to incorrect choices (all post-hoc tests, $p<0.001$), **Figure 4CD**. Thus, ACC inhibition reduced a trial accuracy theta signal during reversal learning in ACC (**Figure 4A** compared to **Figure 4C**), but had no impact on OFC theta. Results plotted by early vs. late reversal revealed a similar pattern (**Figure S4**): there was a main effect of trial type on normalized OFC theta in reversal, whether rats received VEH first [$F(1,52)=37.235$, $p=1.33e^{-07}$] or CNO first [$F(1,70)=17.88$, $p=6.99e^{-05}$]; all Bonferroni corrected post-hoc of correct vs. incorrect trials, $p<0.001$. Though there was the same trend for OFC theta in eGFP animals, this difference

was not statistically significant. Additionally, an analysis of individual rat (not session) changes in normalized theta revealed the same pattern of an attenuated trial accuracy theta signal during reversal learning in ACC, and an intact OFC theta signal of correct vs. incorrect in the hM4Di group (**Figure S5**): [$F(1,15)=20.831$, $p=6.50e^{-04}$]; all Bonferroni corrected post-hoc of correct vs. incorrect trials, $p<0.001$.

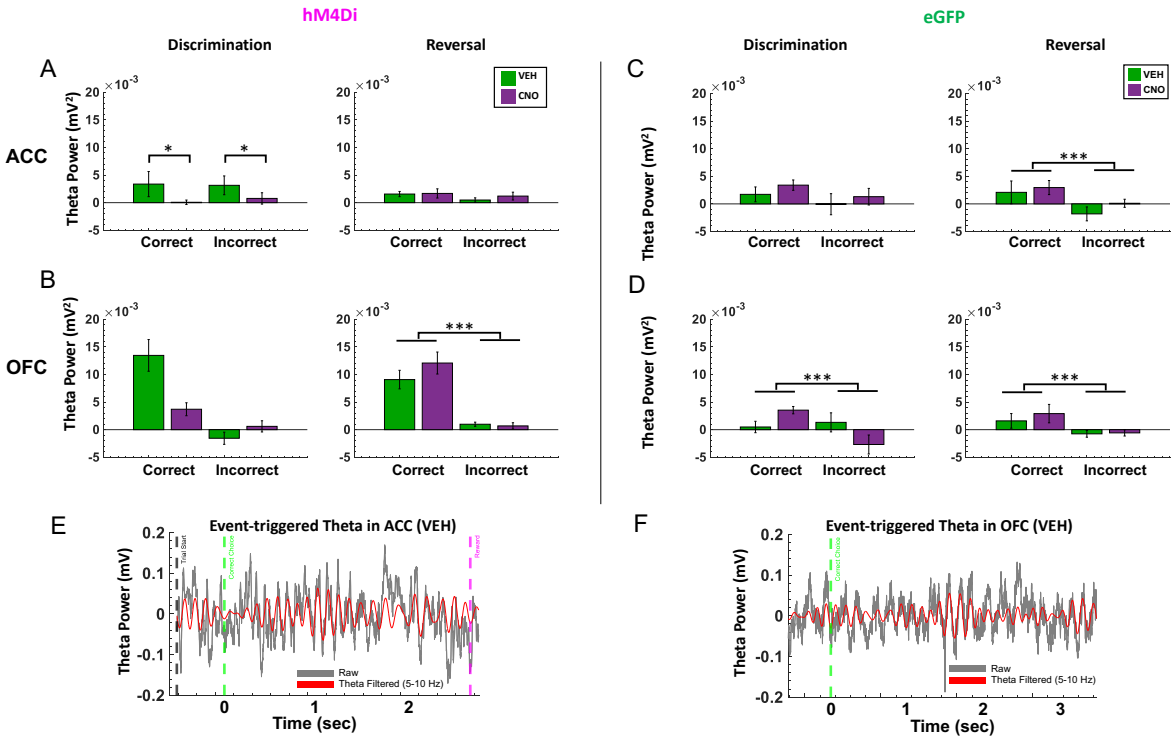

Figure 4. Trial accuracy can be distinguished only from OFC, not ACC, theta power in the reversal phase following ACC inhibition. Baseline-subtracted (normalized) theta power was calculated for correct and incorrect choices in the discrimination and reversal learning phases. (**A**) In hM4Di animals, there was no significant difference in normalized ACC theta power between correct vs. incorrect trials in the reversal phase. (**B**) In hM4Di animals, there was no significant difference in normalized theta power in OFC for correct vs. incorrect trials in discrimination, but normalized theta power in OFC did signal trial accuracy in reversal learning. (**C**) In eGFP animals, normalized theta power in ACC signaled trial accuracy in reversal learning. (**D**) In eGFP animals, normalized theta power in OFC signaled trial accuracy in both discrimination and reversal learning. (**E**) Example event-triggered raw (gray) and theta filtered (red) trace in hM4Di rat with trial start (black dotted line) and correct choice (green dotted line), and reward collection (pink dotted line) denoted for the trial. (**F**) Example event-triggered raw (gray) and theta-filtered (red) trace in eGFP rat with correct choice (green dotted line) denoted for the trial. Means ± standard error of the mean (S.E.M.) bars. ***p<0.001, *p<0.05 following Bonferroni-corrected post-hoc comparisons.

ACC inhibition hastens incorrect choices in reversal learning

Because we were also interested in theta oscillations as they relate to speed of response, we next analyzed median latencies, i.e., to initiate a trial, to choose the correct stimulus, to choose the incorrect stimulus, and to collect reward (Harris, Aguirre et al. 2021) in both discrimination

221 and reversal learning. We focused on measures for which an omnibus across-phase mixed GLM
222 analyses revealed significant phase and drug interactions: *incorrect choice latencies* and *reward*
223 *collection latencies*.

224 In hM4Di animals for the discrimination phase, drug, ACC theta, and OFC theta were not
225 significant predictors of incorrect choice latencies (GLM formula: γ ~ [*1 + Drug*ACCtheta*
226 **OFCtheta + (1+ Drug)*]). However, for the reversal phase, we found a significant effect of drug
227 (β_{drug} =-4.062, t(67)=-2.289, *p*=0.025; VEH slower than CNO, respective means 1.88s vs 1.72s, **Figure**
228 **5A**), and OFC theta, not ACC theta, was a significant predictor of incorrect choice latencies (GLM:
229 $\beta_{OFCtheta}$ =-89.086, t(67)=-2.377, *p*=0.020)**.** For reward collection latencies in the reversal phase, we
230 found a significant effect of drug (GLM: β_{drug} =-4.217, t(67)=-2.081, *p*=0.041; VEH slower than CNO,
231 respective means 0.63s vs 0.52s). We also observed a significant negative correlation between OFC
232 theta power and reward collection speed under CNO (r=-0.14934, *p*=0.031) but not under VEH
233 conditions (r=-0.0071, *p*=0.911). There were no other correlations between theta power and speed
234 in hM4Di rats (**Figure 6**).

235 In eGFP rats, we did not observe significant differences in median latencies when
236 comparing CNO vs. VEH conditions in either the discrimination or reversal phase (**Figure 5B**).
237 Also unlike in hM4Di animals, in eGFP rats there were significant correlations between speed of
238 correct choices (i.e., deliberation speed) and theta power in the VEH, but not CNO, conditions.
239 During post-criterion discrimination performance, OFC theta power was negatively correlated
240 with correct choice (r=-0.13, p=0.02), but not under CNO conditions (r=-0.05, p=0.331). Similarly,
241 ACC theta power was negatively correlated with deliberation speed for correct choices under
242 VEH (r=-0.11, p=0.049), but not under CNO (r=-0.03, p=0.56). In reversal learning, both ACC theta
243 power (r=-0.16, *p*=3.55e-08) and OFC theta power (r=-0.08, *p*=0.01) were negatively correlated with
244 reward collection speed under CNO, but not VEH, conditions (**Figure 7**). We also found a
245 significant drug x phase interaction (GLM: $\beta_{drug\ x\ phase}$ =-3.329, t(65)=-2.301, *p*=0.025) for initiation
246 latencies, however post-hoc analyses did not reveal any statistically significant differences.
247

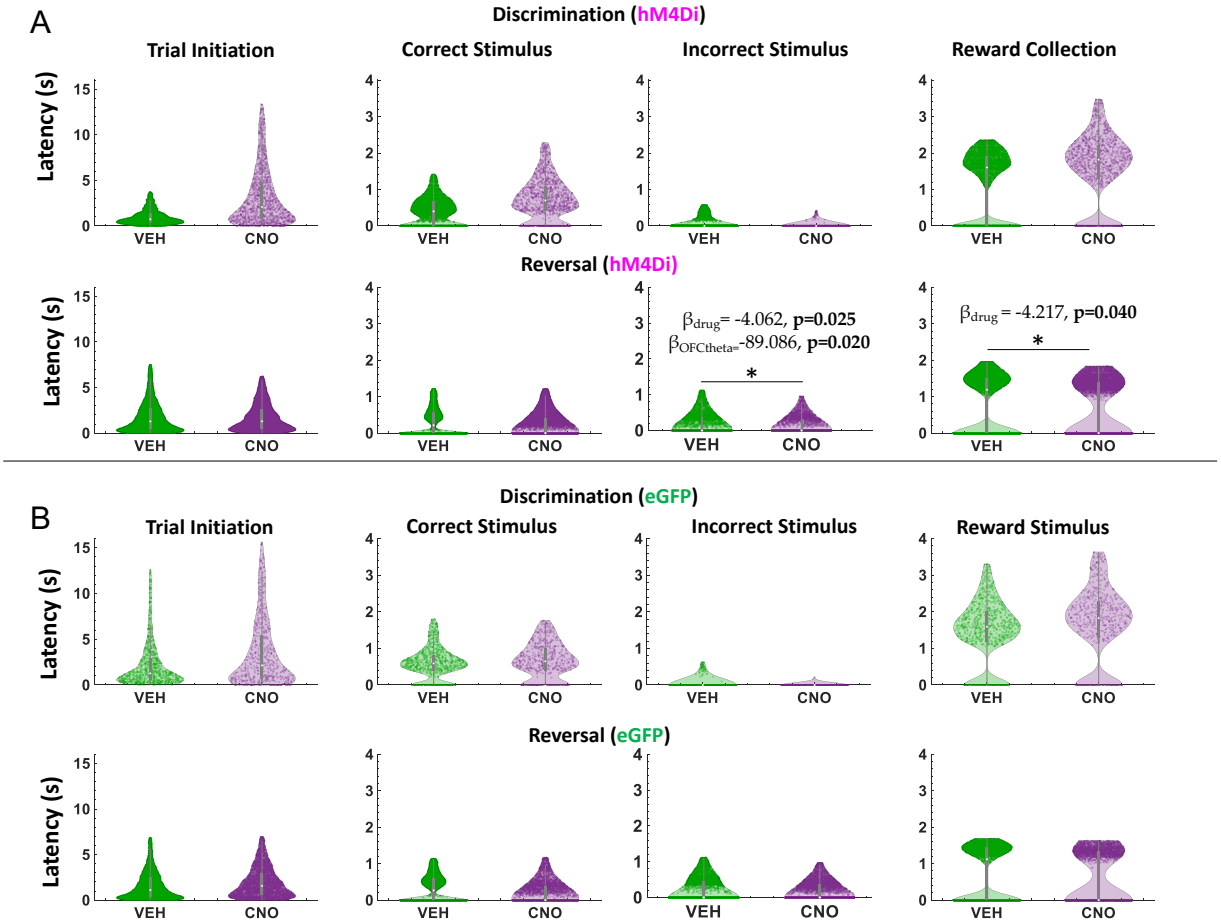

Figure 5. ACC inhibition increases speed of incorrect choices in reversal learning. Violin plots depicting individual trial median latencies in seconds (s) for each of the trial epochs in discrimination and reversal learning for hM4Di and eGFP rats. Individual dots represent trials. (**A**) In hM4Di rats, clozapine-N-oxide (CNO) administration significantly reduced the latency to choose the incorrect stimulus and collect reward in the reversal, not discrimination, phase. ACC theta did not predict speed of responses for any trial epoch in either the discrimination or reversal phase. (**B**) In eGFP rats, there was no significant hastening of incorrect choices, though there was a significant drug x phase interaction for trial initiation latencies (subsequent post-hoc effects were not statistically significant). All significant Beta values are not shown, but are reported in text. *p<0.05, CNO vs. VEH.

Our finding speed-theta power correlations for correct choices in eGFP, and not hM4Di, animals suggest control rats are more certain of correct choices (i.e., faster correct choice, greater theta power) under VEH than under CNO during post-criterion performance, and further, that CNO enhances the relationship between reward collection speed and theta power in OFC of control rats.

Taken together, the latency analyses in learning reveal quicker deliberation speed for incorrect trials during the reversal phase following ACC inhibition. Notably, CNO had an effect on reward collection times in both eGFP and hM4Di animals, with greater theta power in OFC

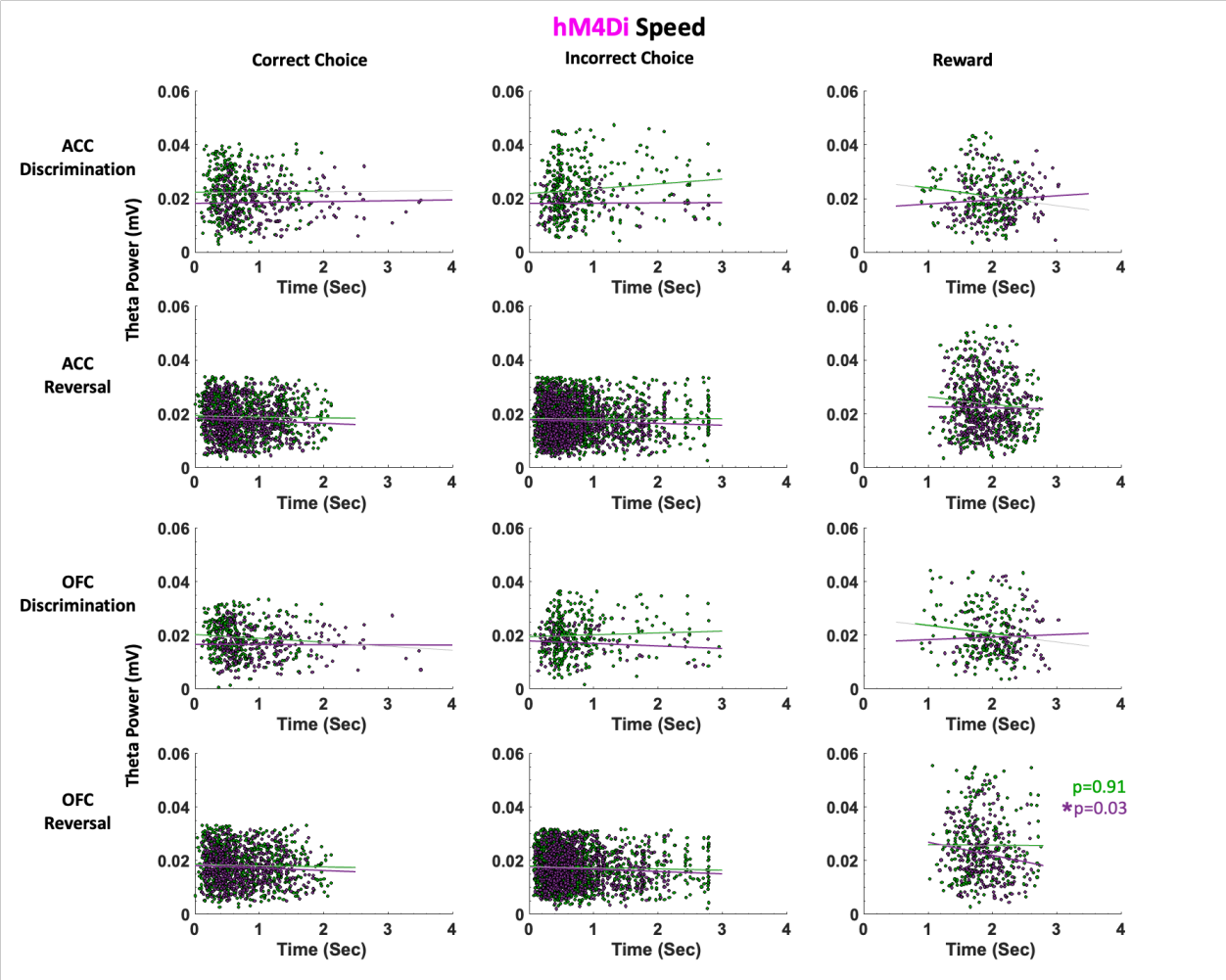

Figure 6. ACC and OFC theta power are not correlated with deliberation speed in either discrimination or reversal learning in hM4Di rats. Theta power was filtered and extracted from ACC and OFC for each event-triggered epoch (Correct choice, Incorrect choice, and Reward port entry). Movement speed was calculated by subtracting the time at the target event (t) from the time at the previous event (t-1) in seconds (Sec). OFC theta power decreased as reward collection latencies increased after CNO administration (purple) during reversal learning. This negative correlation was not observed following VEH (green). There were no significant correlations between theta power and choice of correct or incorrect stimulus. *p<0.05.

265 associated with quicker reward collection times, indicating a drug effect, not an ACC inhibition
266 effect. However, reward collection latencies best indicate motivation levels, not deliberation
267 speed (Harris, Aguirre et al. 2021). We show here that CNO does not produce global locomotor
268 effects which would be reflected across all trial epochs in our task, in contrast to a previous report
269 (MacLaren, Browne et al. 2016).

270

271 ***Theta coherence during correct vs. incorrect trials***

272 Previous studies by other groups have explored the degree to which the ACC and OFC
273 are synchronized during effort- and value-based decisions (Fatahi, Haghparast et al. 2018, Fatahi,
274 Ghorbani et al. 2020), with evidence suggesting significant coherence in the theta-band prior to,
275 and after, making the correct decision. Given that we observed differences in choice accuracy
276 between hM4Di and eGFP animals, coherence analyses during these triggered events could
277 provide a deeper understanding of ACC-OFC theta synchronization. Here, spectral coherence
278 was calculated across trials after aligning the raw local field data from -2 to +2 seconds of the
279 animal's choice, with time=0 indicating the precise time in which the choice was made. Identical
280 to the theta-band filtered data above, the average pre-choice period (-200 to 0 ms) was subtracted
281 from the entire -2 to +2 second window. In the discrimination phase, a 2x2 (drug x virus) ANOVA
282 revealed a significant difference between hM4Di vs. eGFP virus groups in theta coherence during
283 correct choices in the discrimination phase [$F(1,39)=6.538$, $p=0.01$]. However, Bonferroni-corrected
284 post hoc *t*-tests did not result in a significant difference. We did not observe any statistically
285 significant coherence differences for incorrect choices during discrimination phase (**Figure S5**) or
286 for correct or incorrect choices in the reversal phase (**Figure S6**). Thus, we found ACC-OFC theta
287 coherence to be fairly weak in our task despite observing significant differences in theta power
288 during choice accuracy (**Figure 4**).

289

290

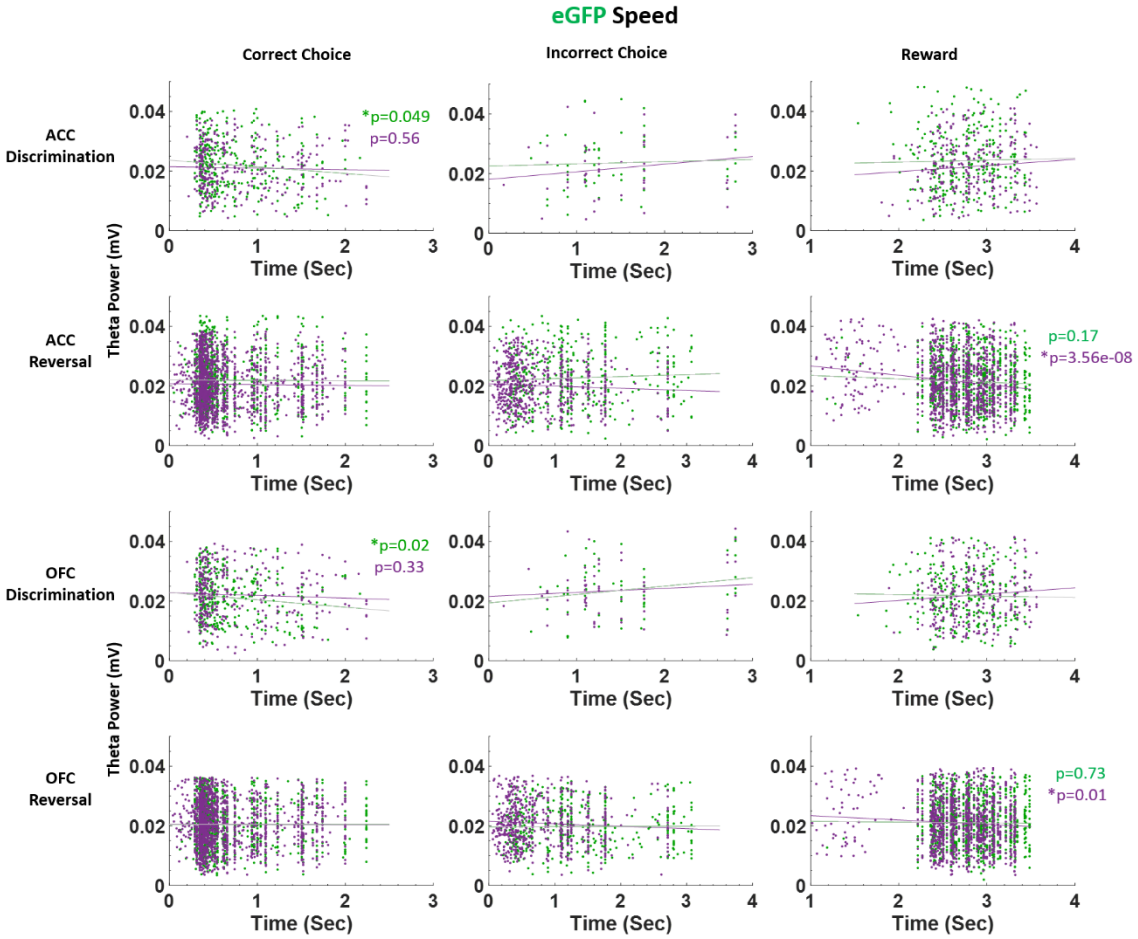

Figure 7. ACC and OFC theta power are negatively correlated with deliberation speed during discrimination performance in eGFP rats. Theta power was filtered and extracted from ACC and OFC for each event-triggered epoch (Correct choice, Incorrect choice, and Reward port entry). Movement speed was calculated by subtracting the time at the target event (t) from the time at the previous event (t-1) in seconds (Sec). OFC theta power decreased as correct choice latencies increased after VEH administration (green) during discrimination learning. This negative correlation was not observed following CNO (purple). In reversal learning, theta power in both ACC and OFC significantly decreased as reward collection latencies increased after CNO administration (purple). This negative correlation was not observed following VEH (green). There were no significant correlations between theta power and choice of correct or incorrect stimulus in reversal learning. *p<0.05.

DISCUSSION

In the present study we were specifically interested in theta oscillations in frontal cortex since there have been several recent reports of involvement of oscillations in this frequency band in reward value and decision making in rodents (Marquardt, Sigdel et al. 2017, Fatahi, Haghparast et al. 2018, Fatahi, Ghorbani et al. 2020, Amarante and Laubach 2021), and one closed-

299 loop experiment in non-human primates demonstrating that theta oscillations in OFC are causally
300 involved in reversal learning (Knudsen and Wallis 2020). We found strong support for OFC theta
301 signaling of accuracy in reversal learning. Theta is a large-scale network oscillation believed to
302 synchronize interregional communication (Buzsaki 2005). The precise origins of OFC theta
303 oscillations are unknown but theta oscillations propagating from the hippocampus to the OFC
304 have been found to encode value learning in macaques (Knudsen and Wallis 2020). While
305 hippocampal theta in rodents is well-established to be associated with certain aspects of
306 movement (Kennedy, Zhou et al. 2022), others have shown that the strength of theta-band phase
307 locking in OFC neurons follows the rat's current outcome expectation, which can be dissociated
308 from licking responses (van Wingerden, Vinck et al. 2010). While volume conduction from the
309 hippocampus is a possibility, the placement of our electrodes in two areas of prefrontal cortex
310 supports a cortical origin for the measured theta oscillations. Previous findings of OFC theta
311 phase locking of spiking patterns also argue against simple hippocampal volume conduction (van
312 Wingerden, Vinck et al. 2010), as well as evidence that ACC coherence with hippocampus is
313 dynamically modulated by behavior, such that ACC theta is not just an attenuated copy of
314 hippocampal theta (Young and McNaughton 2009, Remondes and Wilson 2013).

315 Here we observed a robust OFC theta power signal of accuracy in reversal learning
316 sessions in eGFP and hM4Di animals, unperturbed by ACC inhibition. Since LFPs in OFC, but
317 also broadly in other areas, constitute a composite signal of multiple afferents, it is likely that
318 another input other than ACC is more crucial to the involvement of OFC theta in reversal
319 learning. Additionally, establishing a causal role for oscillations using chemogenetic or other viral
320 approaches is difficult because such manipulations likely disrupt underlying firing rates, a
321 limitation that could be bypassed by a closed-loop approach (Knudsen and Wallis 2020). In
322 particular, the specific silencing of CaMKII projection neurons is not a natural physiological state,
323 and this may trigger compensatory mechanisms in downstream targets that should be
324 investigated in high-yield recording studies in the future.

325 We also analyzed ACC-OFC coherence and found no evidence of significantly enhanced
326 coherence during correct vs. incorrect choices in our task. Other groups have previously utilized

327 a t-maze task that incorporates a spatial component to the decision process, with necessary
328 running both prior to as well as after the choice point in the maze (Fatahi, Haghparast et al. 2018,
329 Fatahi, Ghorbani et al. 2020). While these authors did not determine whether running speed was
330 correlated with ACC-OFC coherence on correct trials, it remains a possibility. High theta
331 coherence between ACC and hippocampus has been associated with coding of an animal's
332 current position during trajectories along a maze that may contribute to decision making
333 (Remondes and Wilson 2013, Remondes and Wilson 2014, Zielinski, Shin et al. 2019). Unlike these
334 maze tasks, movement was much more limited in our task. Indeed, we observed the largest
335 changes in theta power when animals made the choice of the correct stimulus, at which time they
336 were most stationary, just having initiated a trial while fixating on the stimulus. Additionally, we
337 found there were significant increases in speed of incorrect choices following ACC inhibition in
338 the same (reversal) phase when there was no theta 'read-out' of correct vs. incorrect trials. This
339 provides some evidence that ACC inhibition eroded the distinction between correct and incorrect
340 stimuli in the reversal phase, further elaborated below.

341 Various studies, mostly rodent lesion and pharmacological inactivation studies, support
342 the idea that ACC is involved in initial cue or stimulus discrimination learning (Chudasama,
343 Passetti et al. 2003), but has little-to-no involvement in fully-predictive, deterministic reversal
344 learning (Bussey, Muir et al. 1997, Schweimer and Hauber 2006). Conversely, the prediction based
345 on the literature is the opposite for OFC: critical for reversal, but not initial discrimination
346 learning (Schoenbaum, Chiba et al. 1999, Marquardt, Sigdel et al. 2017). Thus, the question about
347 if and how ACC may be causally-involved in stimulus-based reversal learning was a question
348 ripe for investigation. To our knowledge, we are the first to probe this using visual stimuli and
349 with a viral-mediated approach targeting principal neurons in rats. We found that chemogenetic
350 inhibition of ACC indeed impacts reversal learning. The quick adoption of 50% responding is
351 interesting and suggests that animals are either 1) newly satisfied with a 50% reward rate, or 2)
352 unable to distinguish a discrimination vs. reversal 'task state', and thus adopt a random response
353 strategy. The latter possibility is more likely since we found no consistent evidence of
354 motivational changes following ACC inhibition. Labeling of the current task state and building
355 of a cognitive map has been linked to OFC (Wilson, Takahashi et al. 2014, Costa, Scholz et al.

356 2022), yet our data suggest it may also be a role of ACC, at least in rats. The latency data we report
357 here (i.e., demonstrating that animals do not deliberate differently between correct and incorrect
358 stimuli), support this possibility. Surprisingly, we found a drug x virus interaction in reversal
359 learning such that CNO had a dissociable, but non-negligible effect in eGFP reversal learning.
360 Given that this effect of CNO was specific to the late reversal phase and not observed in
361 discrimination learning, it suggests that administration of CNO when performance is at chance
362 may further disrupt reversal learning, given that reversal learning is modulated via a dopamine
363 D2 mechanism (Baldessarini, Centorrino et al. 1993, Lee, Groman et al. 2007, Linden, James et al.
364 2018, Manvich, Webster et al. 2018).

365 As suggested above, theta oscillations in the hippocampus have been shown to correlate
366 with cognitive processing, movement speed and acceleration (Vanderwolf 1969, O'Keefe and
367 Nadel 1978, Kennedy, Zhou et al. 2022). Some evidence suggests theta oscillations in frontal
368 cortex promote inter-regional coordination (Jones and Wilson 2005, Siapas, Lubenov et al. 2005,
369 Cavanagh and Frank 2014, Rajan, Siegel et al. 2019), yet the nature of these relationships is much
370 less firmly established across subregions of frontal cortex. Because our rats are freely-behaving in
371 the operant chambers, we similarly assessed speed of responding at specific trial epochs and
372 correlations with theta power in ACC and OFC. We found that ACC inhibition hastened incorrect
373 choices in reversal learning: this was observed only in hM4Di animals and not in eGFP animals,
374 indicating it was indeed a result of ACC inhibition and not a broad drug effect. In a mixed-effects
375 GLM model with ACC theta, OFC theta, and drug as predictors of latencies, OFC theta and drug
376 (CNO) emerged as the only significant predictors of these quick incorrect choices. In follow-up
377 work, other frequency bands could be systematically probed for speed correlations since not only
378 theta (Fatahi, Haghparast et al. 2018, Fatahi, Ghorbani et al. 2020) but also gamma (Donnelly,
379 Holtzman et al. 2014) oscillations in frontocortical regions have been linked to preparatory motor
380 responses to cues that predict reward. Similarly, beta increases (Schmidt, Herrojo Ruiz et al. 2019)
381 have also been observed at trial-end when working memory engagement is high (in the absence
382 of discrete cues).

383 In summary, the present results suggest a role for ACC in stimulus-based reversal
384 learning; a role similar to that historically proposed for OFC. As several psychiatric conditions

385 manifest impairments in reversal learning including substance use disorder, obsessive
386 compulsive disorder, and schizophrenia (Remijnse, Nielen et al. 2006, Brigman, Ihne et al. 2009,
387 Leeson, Robbins et al. 2009, Winstanley, Olausson et al. 2010, Izquierdo and Jentsch 2012), frontal
388 cortex theta oscillations could be studied as biomarkers in preclinical models of these disorders.
389

390 **MATERIALS AND METHODS**

391 **Animals**

392 A total of N=24 Long-Evans rats (Charles River Laboratories, Hollister, CA) was used for
393 these experiments. Three animals were not included in the final dataset due to implant failure.
394 Six male animals were surgerized to express hM4Di and after three weeks were euthanized
395 shortly after being administered 3 mg/kg of clozapine-N-oxide (CNO), to assess the number of c-
396 fos positive cells in hM4Di-expressing areas versus neighboring (DAPI) areas following vehicle
397 and CNO administration (see details below). Of the n=15 rats used for learning, eight were used
398 for electrophysiological recordings. The latter includes male (*n*=4) and female (*n*=4) animals. All
399 rats were post-natal day 40 (~250g) upon arrival and were pair-housed in a 12-h reverse light/dark
400 cycle room (lights on at 06:00h), maintained in 22-24ºC temperature conditions, with food and
401 water available *ad libitum* prior to behavioral testing. After one week of acclimation to our
402 vivarium, all animals were handled for 10 min in pairs for 5 days. After the handling period,
403 animals were individually-housed to carefully monitor food consumption under restricted
404 access. All procedures shown in the experimental timeline (**Figure 1A**) were in accordance with
405 the recommendations of the Guide for the Care and Use of Laboratory Animals of the National
406 Institutes of Health. The protocol was approved by the Chancellor's Animal Research Committee
407 at the University of California, Los Angeles.

408

409 **Viral Constructs**

410 An adeno-associated virus AAV8 driving the hM4Di-mCherry sequence under the
411 CaMKIIa promoter was used to express DREADDs on putative projection neurons in ACC
412 (*AAV8-CaMKIIa-hM4D(Gi)-mCherry*, packaged by Addgene, Addgene, viral prep #50477-AAV8).
413 A virus lacking the hM4Di DREADD gene and instead containing the fluorescent tag eGFP

414 (*AAV8-CaMKIIa-EGFP*, packaged by Addgene) was infused into ACC in 4 animals as a null virus
415 control. The DREADDs-transfected and null eGFP animals underwent identical surgeries, and all
416 of our behavior was conducted in a counterbalanced within-subject design with each animal
417 serving as its own control (VEH compared to CNO). Collectively, this allowed us to control for
418 non-specific effects of surgical procedures, exposure to AAV8, and non-specific effects of CNO.
419 We note that several recent electrophysiology experiments combining neural recordings with
420 DREADDs do not include virus (eGFP) controls (Liu, McAfee et al. 2017, Alexander, Brown et al.
421 2018, Schmidt, Duin et al. 2019), as we do here.
422

423 **Behavioral Apparatus**

424 Behavioral testing was conducted in operant conditioning chambers shielded for
425 electrophysiological recordings and outfitted with an LCD touchscreen opposing a sucrose pellet
426 dispenser (Lafayette Instrument Co., Lafayette, IN). Sucrose pellets (45mg, Dustless Precision
427 Pellets #F0023, Bio-Serv) were used as rewards. The inner chamber walls were modified to
428 accommodate implanted animals by maximizing the space available (24cm x 33.2cm x 39.5cm)
429 and to improve electrophysiological signal quality. All chamber equipment was controlled by
430 customized ABET II TOUCH software.

431

432 **Pretraining**

433 Immediately following the 5 days of handling, rats were placed on food restriction (12
434 g/d) to no less than 85% of their free-feeding body weight throughout the entire experiment and
435 were weighed each day and monitored closely to not fall below this percentage. Animals were
436 pretrained using the protocol as previously published (Stolyarova and Izquierdo 2017). Briefly, a
437 series of pretraining stages: Habituation, Initiation Touch to Center (ITC), and Immediate Reward
438 (IM), were designed to train rats to nosepoke, initiate a trial, and select a stimulus to obtain a
439 reward.

440 In the habituation stage, five pellets were automatically dispensed and rats were required
441 to consume all pellets within 15 min to advance. In the ITC stage, the center of the touch screen

displayed a white square graphic against a black background. A single sucrose pellet was dispensed with simultaneous onset of audio tone and illumination of the reward receptacle if the rat nosepoked the white stimulus, if rats took longer than 40 s to take this action, the white stimulus disappears without reward and trial was considered an omission followed by a 10 s inter-trial interval (ITI). Rats were required to reach a criterion of consuming 60 rewards in 45 min in order to advance to IM training. In this stage, the same white stimulus was presented as in ITC and a nosepoke indicated trial initiation. The disappearance of the white stimulus was immediately followed by the presentation of a target stimulus on the left or right side of the touchscreen (i.e., forced choice), nose poking this target stimulus was paired with a reward. An *initiation omission* was scored if rats took longer than 40 s to initiate the trial, a *choice omission* was scored if rats failed to nosepoke the left or right stimulus after 60 s. A criterion of 60 rewards consumed in 45 min across two consecutive days was required to advance to the discrimination phase of the behavioral task.

Surgical Procedures

After completing the final pretraining stage, rats were anesthetized with isoflurane for bilateral ACC DREADDS (AAV8-CaMKIIα-hM4D(G_i)-mCherry, Addgene, Cambridge, MA, Addgene, viral prep #50477-AAV8) or eGFP (AAV8-CaMKIIa-EGFP, Addgene, Cambridge, MA, Addgene, viral prep #50469-AAV8) infusion and unilateral chronic implantation of electrode arrays in both ACC and OFC. Craniotomies were created and a 26-gauge guide cannula (PlasticsOne, Roanoke, VA) were lowered into ACC (AP: +3.7, ML: ±0.8, DV: -2.6 from skull surface), after which a 33-gauge internal cannula (PlasticsOne, Roanoke, VA) was inserted. This set of coordinates for ACC was the more anterior site of the two sites that our lab has previously utilized: more posterior ACC has been probed in effort-based tasks (Hart, Blair et al. 2020) whereas stimulus-based reversal learning has been probed with this more anterior targeting (Stolyarova, Rakhshan et al. 2019), constituting area 32 of cingulate cortex (van Heukelum, Mars et al. 2020). Animals were infused with 0.3 μL of virus at a flow rate of 0.1 μL/minute, with cannulae left in place for 5 additional minutes to allow for diffusion.

470 In the same surgery after DREADDs infusion, rats were implanted with a custom-
471 designed 16-channel electrode array manufactured in-house. The array was composed of 8
472 stereotrodes (California Fine Wire Co., Grover Beach, CA) with four targeting the ACC and
473 another four aimed simultaneously in the ipsilateral OFC (AP: +3.7, ML: ±2.0, DV: -4.6, from skull
474 surface), **Figure 3A**. Electrodes were lowered into the same coordinates for ACC as the viral
475 infusions and fixed in place. Stainless steel anchor screws were placed across the skull surface
476 and a ground/reference screw was inserted over the cerebellum. Arrays were secured in place
477 with cyanoacrylate, bone cement (C&B Metabond, Parkell Inc., Edgewood, NY), and dental
478 acrylic (Patterson Dental, St. Paul, MN). Animals were provided with post-operative Carprofen
479 (5 mg/kg, *s.c.*; Zoetis, Parsippany, NJ), topical anti-biotic ointment (Water-Jel Technologies,
480 Carlstadt, NJ) at the incision site, and oral antibiotics (Sulfamethoxazole and trimethoprim oral
481 suspension USP, Pharmaceutical Associates, Inc., Greenville, SC) daily for five days.
482

483 **Drug treatment**

484 Rats were given intraperitoneal (*i.p.*) injections of vehicle (VEH: 95% saline + 5% DMSO)
485 or CNO (3 mg/kg CNO in 95% saline + 5% DMSO) 30 min prior to beginning the behavioral task
486 (Stolyarova, Rakhshan et al. 2019, Hart, Blair et al. 2020). As shown in **Figure 1C**, in the
487 discrimination stage upon reaching 80% correct across two consecutive days without drug, rats
488 performed 4 additional sessions of discrimination learning to test for mastery and successful
489 retention. Sessions 1 and 2 after reaching 80% criterion was performed after a single i.p. CNO
490 injection, and Sessions 3 and 4 after a single i.p. injection of vehicle (VEH). If rats did not continue
491 to reach criterion on Session 4 of VEH, subsequent testing sessions were administered with VEH
492 until the criterion was exceeded after which the reversal stage would commence. Injections of
493 VEH or CNO were administered before every reversal session. Once rats reached 50% correct
494 across two consecutive sessions, the other drug was administered for all subsequent reversal
495 sessions until reaching the 80% criterion. Administration of CNO or VEH for the first half (<50%)
496 and VEH or CNO for the second half (>50%) of reversal sessions was counterbalanced across
497 animals.
498

499 **Stimulus-based discrimination and reversal learning**

500 After one week of post-surgery recovery, rats began the stimulus-based discrimination
501 learning task (**Figure 1B**). This task was described in detail previously (Aguirre, Stolyarova et al.
502 2020, Harris, Aguirre et al. 2021), however, in the present design we assigned deterministic
503 stimulus-reward assignments – correct (100%) vs incorrect (0%). Rats initiated each trial by
504 nosepoking a white graphic stimulus in the center screen (displayed for 40 s). The disappearance
505 of the initiation stimulus was immediately followed by two distinct visual stimuli ('fan' vs.
506 'marbles') presented on the left and right side of the touch screen (displayed for 60 s)
507 pseudorandomly on each trial. One stimulus was paired with a sucrose pellet reward 100% of the
508 time while the other stimulus was not rewarded. Trials that were not initiated within 40 s were
509 scored as an *initiation omission*, whereas failure to select a choice stimulus was scored as a *choice*
510 *omission*. Non-rewarded trials were followed by a 5 s time-out, and all trials including omissions
511 were concluded with a 10 s ITI before commencing the next trial. The overall learning criterion
512 constituted meeting the requirement of consuming 60 or more rewards along with selecting the
513 correct option >80% of the trials within a 60 min session across two consecutive days. As above,
514 upon reaching criterion, rats performed an additional four sessions after receiving an injection of
515 CNO or VEH. Rats would then advance to the reversal phase in which the previously correct
516 stimulus was now the incorrect stimulus. Methods and criterion were identical to those described
517 above. Rats then received injections of VEH or CNO on the first day of reversal, and on reaching
518 50% correct (similarly across 2 days and with 60 or more rewards collected), drug injections were
519 switched until reaching the 80% criterion. Injections of VEH or CNO during the reversal stage
520 was counterbalanced across animals.

521

522 **Electrophysiological Recordings**

523 Local field potential (LFP) data in ACC and OFC were acquired at 30 kHz and down
524 sampled to 1,000 Hz. LFPs were bandpass filtered for theta (5-10 Hz) using the *filtfilt()* function
525 in MATLAB. ACC DREADDs placement and electrodes placement are shown in **Figure 3.** Four
526 behavioral task epochs (e.g., trial initiation, correct choice, incorrect choice, and reward port
527 entry) were configured as triggered event outputs from each operant chamber to the data

528 acquisition system that were simultaneously collected with the electrophysiological recordings.
529 Specific events were averaged over trials and over sessions, and subsequently combined across
530 rats.

531 Data were acquired from a multi-channel data acquisition system (Blackrock
532 Microsystems, LLC., Salt Lake City, UT). The digitizing headstage was connected to the electrode
533 array, and signal was sent to the recording system through a tether and commutator (Dragonfly
534 Inc. Ridgeley, WV). Recording sessions were conducted on all behavioral sessions preceded by
535 an injection. Neural recordings began 15 min after drug injection followed by a 15 min baseline
536 while the animal was inside the operant chamber. The behavioral task commenced at the end of
537 baseline, a total of 30 min post-injection. Recording data for EGFP control animals for all trial
538 epochs are shown in **Figure S3**.

539

540 **Histology**

541 At the conclusion of the experiment, rats were anesthetized and administered electrolytic
542 lesions at the recording sites via direct current stimulation (20 μA for 20 s), **Figure 3A**. Rats were
543 euthanized 3 days later by sodium pentobarbital (Euthasol, 0.8 mL, *i.p.*; Virbac, Fort Worth, TX)
544 and brains were extracted via transcardial perfusion with phosphate buffered saline (PBS)
545 followed by 10% buffered formalin acetate and post-fixed in this solution for 24 hours followed
546 by 30% sucrose cryoprotection. Tissue was prepared in 40-μM thick coronal sections and either
547 Nissl stained for verification of electrode placement (**Figure 3B**) or cover slipped with DAPI
548 mounting medium (Prolong gold, Invitrogen, Carlsbad, CA) and amplified with NMDAR1
549 Polyclonal Antibodies (Invitrogen for Thermo Fischer Scientific) for DREADDs verification,
550 visualized using a BZ-X710 microscope (Keyence, Itasca, IL), and analyzed with BZ-X Viewer
551 software. DREADDs expression (visualized by magenta fluorescence) was determined by
552 matching histological sections to a standard rat brain atlas (Paxinos and Watson 2007), **Figure 3C**.

553

554 **c-fos immunohistochemistry**

555 Forty μm coronal sections containing ACC were first incubated overnight (16-18 hours) at 4°C in
556 solution containing primary anti-cfos antibody (Anti-cfos (rabbit), 1:500, Abcam, Cambridge,

557 MA, Catalog Number: ab209794), 10% normal goat serum (Abcam, Cambridge, MA, Cat. #
558 ab7481), and 0.5% Triton-X (Sigma, St. Louis, MO, Cat. # T8787) in 1X PBS, followed by three 10-
559 min washes in PBS. The tissue was then incubated for 4 hours in solution containing 1X PBS,
560 Triton-X and a secondary antibody (Goat anti-Rabbit IgG (H+L), Alexa Fluor® 488 conjugate,
561 1:400, Fisher Scientific, Catalog #A-11034), followed by three 10-min washes in PBS. Slides were
562 subsequently mounted and cover-slipped with DAPI mounting medium (Prolong gold,
563 Invitrogen, Carlsbad, CA), visualized using a BZ-X710 microscope (Keyence, Itasca, IL), and
564 analyzed with BZ-X Viewer software. To verify DREADD-mediated inhibition of neurons in ACC
565 we compared the number of c-fos positive cells in the hM4Di-expressing regions to the number
566 of c-fos positive cells in neighboring (non-hM4Di-expressing, DAPI) areas following vehicle and
567 CNO administration (**Figure 3DE**). Four coronal sections per condition were obtained:
568 hM4Di+VEH, hM4Di+CNO, DAPI+VEH, and DAPI+CNO. There were fewer c-fos positive cells
569 in hM4Di-expressing cells following CNO compared to VEH ($F(1,5)=8.18$, $p=0.049$), but not in
570 DAPI-expressing cells ($F(1,5)=0.02$, $p=0.903$). The difference in c-fos positive cells was not due to
571 sampling differences: the hM4Di-expressing area was not significantly different from the non-
572 hM4Di-expressing (DAPI) area ($t(10)=-1.536$, $p=0.156$).
573

574 **Spectral power and Coherence**

575 Local field potential (LFP) data were acquired at 30 kHz and downsampled to 1,000 Hz.
576 Traces were analyzed for signal artifacts through visual inspection and automatic artifact
577 detection in MATLAB. LFP signals that exceeded absolute value of 1.5 mV or when summed
578 cross-band power (2 – 120 Hz) exceeded the 99.98th percentile, were identified as artifact and
579 excluded from all analyses.

580 Spectral power across frequency bands were determined through a fast Fourier transform
581 via the *spectrogram()* function in MATLAB [frequency bin = 0.5 Hz, 10 s Hanning window]. LFP
582 Coherence (magnitude-squared coherence) was calculated using Welch's averaged modified
583 periodogram method with a 1-s window and a frequency resolution of 1 Hz via MATLAB
584 function *mscohere()*. LFPs were band-pass filtered for theta (5-10 Hz) using the *filtfilt()* function in
585 MATLAB and designed using the *designfilt()* function (stop bands: 2 Hz, 15Hz; pass bands: 5Hz,

586 10Hz). Band-passed theta traces were synchronized from -2 to +2 seconds to each of the four
587 behavioral task triggered events (see Data Analysis) in preparation for analyses. Once aligned,
588 the baseline mean (-200 to 0 ms period preceding the triggered event) was subtracted from time=0
589 to +2 seconds post-event for normalization. Normalized theta for accuracy trail epochs is shown
590 in **Figure S2** and **Figure S3**. ACC-OFC coherence for discrimination and reversal learning is
591 shown in **Figure S5** and **Figure S6**.
592

593 **Data analysis**

594 All behavioral and neurophysiological analyses were performed via custom-written code
595 in MATLAB (MathWorks, Inc., Natick, MA). We first demarcated 4 unique task triggered events
596 for our analyses: 1) trial initiation (center stimulus) nosepoke, 2) nosepoke to S+ (correct stimulus
597 or action), 3) nosepoke to S- (incorrect stimulus or action), and 4) reward collection (food
598 magazine head entry).

599 Learning and performance (speed/latency) data were analyzed with a series of mixed-
600 effects General Linear Models (GLMs) (*fitglme* function; Statistics and Machine Learning Toolbox)
601 first in omnibus analyses that included all factors and both learning phases (discrimination and
602 reversal). For sessions to reach criterion in initial visual discrimination (when animals were not
603 administered drug or recorded), we conducted an independent samples t-test to assess viral
604 group differences. For theta power analyses, 2 x 2 ANOVAs were conducted on baseline-
605 subtracted ACC and OFC theta power with drug (CNO, VEH) x trial type (correct, incorrect) as
606 factors on data averaged from each session. Analyses using trial phase in this case was not treated
607 as a within-subject variable as drug experience differed in each phase: animals received the same
608 order of drug in discrimination (CNO first, then VEH), but drug order was counterbalanced in
609 the reversal phase. Then, each learning phase was analyzed separately for measures where
610 significant interactions of phase were observed. All post-hoc tests were corrected for the number
611 of comparisons (Bonferroni). Statistical significance was noted when p-values were less than 0.05.

612 Major dependent variables included: percent correct (and correct and incorrect choices,
613 probed separately) and median latencies (to initiate a trial, to make the correct choice, to make
614 the incorrect choice, and to collect reward). Pearson correlations for latency measures and theta

power were generated using the *corrcoef* function in MATLAB. Latency datapoints exceeding 2 SD were excluded. For latency values, time at trial event (t=0) was subtracted from the previous trial event (t-1). For example, correct or incorrect choice speed was calculated by subtracting time of choice from time of trial initiation, and reward collection speed was calculated by subtracting time of reward collection from time of correct or incorrect choice, in seconds (sec).

To confirm DREADDs efficacy, the number of c-fos positive cells by different drug conditions (CNO, VEH) in hM4Di-expressing cells and in non-hM4Di expressing cells were analyzed with one-way ANOVAs. To ensure that c-fos positive cells differences were not due to differences in sampling of tissue during microscopy, the area of hM4Di spread of virus was compared to that of non-hM4Di (DAPI) and analyzed using an independent samples t-test.

Conflict of Interest: The authors declare no competing financial interests

Table 1. *Probability of choosing correctly during initial visual discrimination learning*

Discrimination Learning γ = probability of choosing correctly							
Formula	γ ~ [1 + Drug*Session*Virus*Sex + (1 + Session | Rat)]						
Coefficients	**β**	SE	tStat	DF	p	CI_L	CI_U
intercept	0.75869	0.099232	7.6456	102	<.0001	0.56186	0.95551
virus	-0.11377	0.13422	-0.84767	102	0.3986	-0.38	0.15245
drug	0.063004	0.11011	0.57218	102	0.56846	-0.1554	0.28141
sex	-0.061102	0.24282	-0.25163	102	0.80183	-0.54274	0.42053
session	-0.056029	0.011205	-5.0005	102	**<.0001**	-0.07825	-0.03381
virus:drug	-0.032214	0.13606	-0.23677	102	0.81331	-0.30208	0.23765
virus:sex	0.12814	0.34095	0.37584	102	0.70782	-0.54813	0.80441
drug:sex	-0.13438	0.23738	-0.56609	102	0.57257	-0.60523	0.33646
virus:session	0.057054	0.016538	3.4499	102	**<.0001**	0.024251	0.089856
drug:session	0.04231	0.036765	1.1508	102	0.2525	-0.03061	0.11523
sex:session	0.019448	0.12817	0.15173	102	0.8797	-0.23478	0.27368
virus:drug:sex	-0.056662	0.35259	-0.1607	102	0.87265	-0.75603	0.64271
virus:drug:session	-0.081474	0.039519	-2.0617	102	**0.041783**	-0.15986	-0.00309
virus:sex:session	0.041715	0.18132	0.23006	102	0.81851	-0.31794	0.40137
drug:sex:session	-0.029413	0.13287	-0.22138	102	0.82524	-0.29295	0.23412
virus:drug:sex:session	0.12467	0.1982	0.62903	102	0.53074	-0.26845	0.51779

632 **Table 2**. *Probability of choosing correctly during reversal learning*

Reversal Learning γ = probability of choosing correctly							
Formula	γ ~ [1 + Drug*Session*Virus*Sex + (1 + Session| Rat)]						
Coefficients	**β**	SE	tStat	DF	p	CI_L	CI_U
intercept	0.54469	0.077476	7.0305	178	<.0001	0.39181	0.69758
virus	-0.20762	0.098646	-2.1047	178	**0.03672**	-0.40229	-0.01296
drug	-0.15706	0.078148	-2.0997	178	**0.045969**	-0.31127	-0.00284
sex	-0.31948	0.10221	-3.1258	178	**0.002072**	-0.52118	-0.11778
session	-0.005608	0.019074	-0.29403	178	0.76908	-0.04325	0.032032
virus:drug	0.26232	0.10267	2.5549	178	**0.011459**	0.059706	0.46493
virus:sex	0.24254	0.13747	1.7642	178	0.079411	-0.02876	0.51383
drug:sex	0.29399	0.10467	2.8087	178	**0.005529**	0.087436	0.50054
virus:session	0.031054	0.020933	1.4835	178	0.1397	-0.01025	0.072363
drug:session	0.015992	0.019692	0.8121	178	0.41782	-0.02287	0.054851
sex:session	0.039986	0.020312	1.9686	178	0.050556	-9.79e-05	0.080069
virus:drug:sex	-0.2572	0.1476	-1.7425	178	0.083141	-0.5485	0.034072
virus:drug:session	-0.035597	0.023011	-1.547	178	0.12365	-0.08101	0.009812
virus:sex:session	-0.032032	0.023057	-1.3893	178	0.16649	-0.07753	0.013468
drug:sex:session	-0.027893	0.021945	-1.271	178	0.20537	-0.0712	0.015413
virus:drug:sex:session	0.05759	0.028689	1.9959	178	**0.047474**	0.000645	0.11387

633

634

635

636

637 **REFERENCES**

638 Aguirre, C. G., A. Stolyarova, K. Das, S. Kolli, V. Marty, L. Ray, I. Spigelman and A.
639 Izquierdo (2020). "Sex-dependent effects of chronic intermittent voluntary alcohol consumption
640 on attentional, not motivational, measures during probabilistic learning and reversal." PLoS
641 One **15**(6): e0234729.
642 Akam, T., I. Rodrigues-Vaz, I. Marcelo, X. Zhang, M. Pereira, R. F. Oliveira, P. Dayan
643 and R. M. Costa (2021). "The Anterior Cingulate Cortex Predicts Future States to Mediate
644 Model-Based Action Selection." Neuron **109**(1): 149-163 e147.
645 Alexander, G. M., L. Y. Brown, S. Farris, D. Lustberg, C. Pantazis, B. Gloss, N. W.
646 Plummer, P. Jensen and S. M. Dudek (2018). "CA2 neuronal activity controls hippocampal low
647 gamma and ripple oscillations." Elife **7**.
648 Amarante, L. M. and M. Laubach (2021). "Coherent theta activity in the medial and
649 orbital frontal cortices encodes reward value." eLife **10:e63372**.
650 Baldessarini, R. J., F. Centorrino, J. G. Flood, S. A. Volpicelli, D. Huston-Lyons and B. M.
651 Cohen (1993). "Tissue concentrations of clozapine and its metabolites in the rat."
652 Neuropsychopharmacology **9**(2): 117-124.
653 Barreiros, I. V., M. C. Panayi and M. E. Walton (2021). "Organization of Afferents along
654 the Anterior-posterior and Medial-lateral Axes of the Rat Orbitofrontal Cortex." Neuroscience
655 **460**: 53-68.
656 Boulougouris, V., J. W. Dalley and T. W. Robbins (2007). "Effects of orbitofrontal,
657 infralimbic and prelimbic cortical lesions on serial spatial reversal learning in the rat." Behav
658 Brain Res **179**(2): 219-228.
659 Brigman, J. L., J. Ihne, L. M. Saksida, T. J. Bussey and A. Holmes (2009). "Effects of
660 Subchronic Phencyclidine (PCP) Treatment on Social Behaviors, and Operant Discrimination
661 and Reversal Learning in C57BL/6J Mice." Front Behav Neurosci **3**: 2.
662 Bussey, T. J., J. L. Muir, B. J. Everitt and T. W. Robbins (1997). "Triple dissociation of
663 anterior cingulate, posterior cingulate, and medial frontal cortices on visual discrimination tasks
664 using a touchscreen testing procedure for the rat." Behav Neurosci **111**(5): 920-936.
665 Buzsaki, G. (2005). "Theta rhythm of navigation: link between path integration and
666 landmark navigation, episodic and semantic memory." Hippocampus **15**(7): 827-840.
667 Camille, N., A. Tsuchida and L. K. Fellows (2011). "Double dissociation of stimulus-
668 value and action-value learning in humans with orbitofrontal or anterior cingulate cortex
669 damage." J Neurosci **31**(42): 15048-15052.
670 Cavanagh, J. F. and M. J. Frank (2014). "Frontal theta as a mechanism for cognitive
671 control." Trends Cogn Sci **18**(8): 414-421.
672 Chudasama, Y., F. Passetti, S. E. Rhodes, D. Lopian, A. Desai and T. W. Robbins (2003).
673 "Dissociable aspects of performance on the 5-choice serial reaction time task following lesions of
674 the dorsal anterior cingulate, infralimbic and orbitofrontal cortex in the rat: differential effects
675 on selectivity, impulsivity and compulsivity." Behav Brain Res **146**(1-2): 105-119.
676 Chudasama, Y. and T. W. Robbins (2003). "Dissociable contributions of the orbitofrontal
677 and infralimbic cortex to pavlovian autoshaping and discrimination reversal learning: further
678 evidence for the functional heterogeneity of the rodent frontal cortex." J Neurosci **23**(25): 8771-
679 8780.

Costa, K. M., R. Scholz, K. Lloyd, P. Moreno-Castilla, M. P. H. Gardner, P. Dayan and G. Schoenbaum (2022). "The role of the lateral orbitofrontal cortex in creating cognitive maps." Nat Neurosci.

Cowen, S. L., G. A. Davis and D. A. Nitz (2012). "Anterior cingulate neurons in the rat map anticipated effort and reward to their associated action sequences." J Neurophysiol **107**(9): 2393-2407.

Dalton, G. L., N. Y. Wang, A. G. Phillips and S. B. Floresco (2016). "Multifaceted Contributions by Different Regions of the Orbitofrontal and Medial Prefrontal Cortex to Probabilistic Reversal Learning." J Neurosci **36**(6): 1996-2006.

Donnelly, N. A., T. Holtzman, P. D. Rich, A. J. Nevado-Holgado, A. B. Fernando, G. Van Dijck, T. Holzhammer, O. Paul, P. Ruther, O. Paulsen, T. W. Robbins and J. W. Dalley (2014). "Oscillatory activity in the medial prefrontal cortex and nucleus accumbens correlates with impulsivity and reward outcome." PLoS One **9**(10): e111300.

Fatahi, Z., A. Ghorbani, M. Ismail Zibaii and A. Haghparast (2020). "Neural synchronization between the anterior cingulate and orbitofrontal cortices during effort-based decision making." Neurobiol Learn Mem **175**: 107320.

Fatahi, Z., A. Haghparast, A. Khani and M. Kermani (2018). "Functional connectivity between anterior cingulate cortex and orbitofrontal cortex during value-based decision making." Neurobiol Learn Mem **147**: 74-78.

Groman, S. M., C. Keistler, A. J. Keip, E. Hammarlund, R. J. DiLeone, C. Pittenger, D. Lee and J. R. Taylor (2019). "Orbitofrontal Circuits Control Multiple Reinforcement-Learning Processes." Neuron **103**(4): 734-746 e733.

Harris, C., C. G. Aguirre, S. Kolli, K. Das, A. Izquierdo and A. Soltani (2021). "Unique features of stimulus-based probabilistic reversal learning." Behavioral Neuroscience **135**(4): 550-570.

Hart, E. E., G. J. Blair, T. J. O'Dell, H. T. Blair and A. Izquierdo (2020). "Chemogenetic Modulation and Single-Photon Calcium Imaging in Anterior Cingulate Cortex Reveal a Mechanism for Effort-Based Decisions." J Neurosci **40**(29): 5628-5643.

Hoover, W. B. and R. P. Vertes (2011). "Projections of the medial orbital and ventral orbital cortex in the rat." J Comp Neurol **519**(18): 3766-3801.

Hunt, L. T. and B. Y. Hayden (2017). "A distributed, hierarchical and recurrent framework for reward-based choice." Nat Rev Neurosci **18**(3): 172-182.

Hunt, L. T., W. M. N. Malalasekera, A. O. de Berker, B. Miranda, S. F. Farmer, T. E. J. Behrens and S. W. Kennerley (2018). "Triple dissociation of attention and decision computations across prefrontal cortex." Nat Neurosci **21**(10): 1471-1481.

Hyman, J. M., C. B. Holroyd and J. K. Seamans (2017). "A Novel Neural Prediction Error Found in Anterior Cingulate Cortex Ensembles." Neuron **95**(2): 447-456 e443.

Izquierdo, A., C. Darling, N. Manos, H. Pozos, C. Kim, S. Ostrander, V. Cazares, H. Stepp and P. H. Rudebeck (2013). "Basolateral amygdala lesions facilitate reward choices after negative feedback in rats." J Neurosci **33**(9): 4105-4109.

Izquierdo, A. and J. D. Jentsch (2012). "Reversal learning as a measure of impulsive and compulsive behavior in addictions." Psychopharmacology (Berl) **219**(2): 607-620.

722 Jendryka, M., M. Palchaudhuri, D. Ursu, B. van der Veen, B. Liss, D. Katzel, W. Nissen
723 and A. Pekcec (2019). "Pharmacokinetic and pharmacodynamic actions of clozapine-N-oxide,
724 clozapine, and compound 21 in DREADD-based chemogenetics in mice." Sci Rep **9**(1): 4522.
725 Jones, M. W. and M. A. Wilson (2005). "Theta rhythms coordinate hippocampal-
726 prefrontal interactions in a spatial memory task." PLoS Biol **3**(12): e402.
727 Kennedy, J. P., Y. Zhou, Y. Qin, S. D. Lovett, A. Sheremet, S. N. Burke and A. P. Maurer
728 (2022). "A Direct Comparison of Theta Power and Frequency to Speed and Acceleration." J
729 Neurosci **42**(21): 4326-4341.
730 Knudsen, E. B. and J. D. Wallis (2020). "Closed-Loop Theta Stimulation in the
731 Orbitofrontal Cortex Prevents Reward-Based Learning." Neuron **106**(3): 537-547 e534.
732 Lee, B., S. Groman, E. D. London and J. D. Jentsch (2007). "Dopamine D2/D3 receptors
733 play a specific role in the reversal of a learned visual discrimination in monkeys."
734 Neuropsychopharmacology **32**(10): 2125-2134.
735 Leeson, V. C., T. W. Robbins, E. Matheson, S. B. Hutton, M. A. Ron, T. R. Barnes and E.
736 M. Joyce (2009). "Discrimination learning, reversal, and set-shifting in first-episode
737 schizophrenia: stability over six years and specific associations with medication type and
738 disorganization syndrome." Biol Psychiatry **66**(6): 586-593.
739 Linden, J., A. S. James, C. McDaniel and J. D. Jentsch (2018). "Dopamine D2 Receptors in
740 Dopaminergic Neurons Modulate Performance in a Reversal Learning Task in Mice." eNeuro
741 **5**(1).
742 Liu, Y., S. S. McAfee and D. H. Heck (2017). "Hippocampal sharp-wave ripples in awake
743 mice are entrained by respiration." Sci Rep **7**(1): 8950.
744 Luk, C. H. and J. D. Wallis (2013). "Choice coding in frontal cortex during stimulus-
745 guided or action-guided decision-making." J Neurosci **33**(5): 1864-1871.
746 MacLaren, D. A., R. W. Browne, J. K. Shaw, S. Krishnan Radhakrishnan, P. Khare, R. A.
747 Espana and S. D. Clark (2016). "Clozapine N-Oxide Administration Produces Behavioral Effects
748 in Long-Evans Rats: Implications for Designing DREADD Experiments." eNeuro **3**(5).
749 Manvich, D. F., K. A. Webster, S. L. Foster, M. S. Farrell, J. C. Ritchie, J. H. Porter and D.
750 Weinshenker (2018). "The DREADD agonist clozapine N-oxide (CNO) is reverse-metabolized to
751 clozapine and produces clozapine-like interoceptive stimulus effects in rats and mice." Sci Rep
752 **8**(1): 3840.
753 Marquardt, K., R. Sigdel and J. L. Brigman (2017). "Touch-screen visual reversal learning
754 is mediated by value encoding and signal propagation in the orbitofrontal cortex." Neurobiol
755 Learn Mem **139**: 179-188.
756 Mashhoori, A., S. Hashemnia, B. L. McNaughton, D. R. Euston and A. J. Gruber (2018).
757 "Rat anterior cingulate cortex recalls features of remote reward locations after disfavoured
758 reinforcements." Elife **7**.
759 O'Keefe, J. and L. Nadel (1978). The hippocampus as a cognitive map. New York,
760 Clarendon Press; Oxford University Press.

761 Paxinos, G. and C. Watson (2007). The rat brain in stereotaxic coordinates. Amsterdam ;
762 Boston ;, Academic Press/Elsevier.

Rajan, A., S. N. Siegel, Y. Liu, J. Bengson, G. R. Mangun and M. Ding (2019). "Theta Oscillations Index Frontal Decision-Making and Mediate Reciprocal Frontal-Parietal Interactions in Willed Attention." Cereb Cortex **29**(7): 2832-2843.

Remijnse, P. L., M. M. Nielen, A. J. van Balkom, D. C. Cath, P. van Oppen, H. B. Uylings and D. J. Veltman (2006). "Reduced orbitofrontal-striatal activity on a reversal learning task in obsessive-compulsive disorder." Arch Gen Psychiatry **63**(11): 1225-1236.

Remondes, M. and M. A. Wilson (2013). "Cingulate-hippocampus coherence and trajectory coding in a sequential choice task." Neuron **80**(5): 1277-1289.

Remondes, M. and M. A. Wilson (2014). "Cingulate-Hippocampus Coherence and Trajectory Coding in a Sequential Choice Task." Neuron **81**(5): 1214.

Riceberg, J. S. and M. L. Shapiro (2012). "Reward stability determines the contribution of orbitofrontal cortex to adaptive behavior." J Neurosci **32**(46): 16402-16409.

Rudebeck, P. H., T. E. Behrens, S. W. Kennerley, M. G. Baxter, M. J. Buckley, M. E. Walton and M. F. Rushworth (2008). "Frontal cortex subregions play distinct roles in choices between actions and stimuli." J Neurosci **28**(51): 13775-13785.

Rudebeck, P. H. and A. Izquierdo (2021). "Foraging with the frontal cortex: A cross-species evaluation of reward-guided behavior." Neuropsychopharmacology.

Rudebeck, P. H., M. E. Walton, A. N. Smyth, D. M. Bannerman and M. F. Rushworth (2006). "Separate neural pathways process different decision costs." Nat Neurosci **9**(9): 1161-1168.

Schmidt, B., A. A. Duin and A. D. Redish (2019). "Disrupting the medial prefrontal cortex alters hippocampal sequences during deliberative decision making." J Neurophysiol **121**(6): 1981-2000.

Schmidt, R., M. Herrojo Ruiz, B. E. Kilavik, M. Lundqvist, P. A. Starr and A. R. Aron (2019). "Beta Oscillations in Working Memory, Executive Control of Movement and Thought, and Sensorimotor Function." J Neurosci **39**(42): 8231-8238.

Schoenbaum, G., A. A. Chiba and M. Gallagher (1999). "Neural encoding in orbitofrontal cortex and basolateral amygdala during olfactory discrimination learning." J Neurosci **19**(5): 1876-1884.

Schweimer, J. and W. Hauber (2006). "Dopamine D1 receptors in the anterior cingulate cortex regulate effort-based decision making." Learn Mem **13**(6): 777-782.

Siapas, A. G., E. V. Lubenov and M. A. Wilson (2005). "Prefrontal phase locking to hippocampal theta oscillations." Neuron **46**(1): 141-151.

Stolyarova, A. and A. Izquierdo (2017). "Complementary contributions of basolateral amygdala and orbitofrontal cortex to value learning under uncertainty." Elife **6**.

Stolyarova, A., M. Rakhshan, E. E. Hart, T. J. O'Dell, M. A. K. Peters, H. Lau, A. Soltani and A. Izquierdo (2019). "Contributions of anterior cingulate cortex and basolateral amygdala to decision confidence and learning under uncertainty." Nat Commun **10**(1): 4704.

van Heukelum, S., R. B. Mars, M. Guthrie, J. K. Buitelaar, C. F. Beckmann, P. H. E. Tiesinga, B. A. Vogt, J. C. Glennon and M. N. Havenith (2020). "Where is Cingulate Cortex? A Cross-Species View." Trends Neurosci **43**(5): 285-299.

van Wingerden, M., M. Vinck, J. Lankelma and C. M. Pennartz (2010). "Theta-band phase locking of orbitofrontal neurons during reward expectancy." J Neurosci **30**(20): 7078-7087.

Vanderwolf, C. H. (1969). "Hippocampal electrical activity and voluntary movement in the rat." Electroencephalogr Clin Neurophysiol **26**(4): 407-418.

Wilson, R. C., Y. K. Takahashi, G. Schoenbaum and Y. Niv (2014). "Orbitofrontal cortex as a cognitive map of task space." Neuron **81**(2): 267-279.

Winstanley, C. A., P. Olausson, J. R. Taylor and J. D. Jentsch (2010). "Insight into the relationship between impulsivity and substance abuse from studies using animal models." Alcohol Clin Exp Res **34**(8): 1306-1318.

Young, C. K. and N. McNaughton (2009). "Coupling of theta oscillations between anterior and posterior midline cortex and with the hippocampus in freely behaving rats." Cereb Cortex **19**(1): 24-40.

Zielinski, M. C., J. D. Shin and S. P. Jadhav (2019). "Coherent Coding of Spatial Position Mediated by Theta Oscillations in the Hippocampus and Prefrontal Cortex." J Neurosci **39**(23): 4550-4565.